RESEARCH ARTICLE

CLINICAL MEDICINE

10.1126/sciadv.1500973

Pharmacologic inhibition of JAK-STAT signaling promotes hair growth

Sivan Harel,[1] Claire A. Higgins,[1]* Jane E. Cerise,[1] Zhenpeng Dai,[1] James C. Chen,[1,2] Raphael Clynes,[1] Angela M. Christiano[1,3]†

Several forms of hair loss in humans are characterized by the inability of hair follicles to enter the growth phase (anagen) of the hair cycle after being arrested in the resting phase (telogen). Current pharmacologic therapies have been largely unsuccessful in targeting pathways that can be selectively modulated to induce entry into anagen. We show that topical treatment of mouse and human skin with small-molecule inhibitors of the Janus kinase (JAK)–signal transducer and activator of transcription (STAT) pathway results in rapid onset of anagen and subsequent hair growth. We show that JAK inhibition regulates the activation of key hair follicle populations such as the hair germ and improves the inductivity of cultured human dermal papilla cells by controlling a molecular signature enriched in intact, fully inductive dermal papillae. Our findings open new avenues for exploration of JAK-STAT inhibition for promotion of hair growth and highlight the role of this pathway in regulating the activation of hair follicle stem cells.

INTRODUCTION

Several hair growth disorders are characterized by the inability to re-enter the growth phase of the hair cycle (anagen) due to hair follicle (HF) miniaturization in the case of androgenetic alopecia or immune dysfunction in the case of alopecia areata (AA). Current pharmacological therapy for androgenetic alopecia is primarily focused on the prevention of further hair loss. However, the search for pharmacologic agents to restart the hair cycle has been largely unsatisfactory. Recently, we demonstrated that pharmacological inhibition of the Janus kinase (JAK)–signal transducer and activator of transcription (STAT) pathway promotes rapid hair regrowth in AA in both mice and humans (*1*). Unexpectedly, during the course of our studies on mice with AA, we observed that topical treatment with JAK-STAT inhibitors resulted in an unusually robust hair growth, suggesting a localized effect on initiation of the hair cycle. Here, we show that pharmacological inhibition of JAK-STAT signaling initiates the hair cycle in normal mice and promotes growth of hair follicles in humans.

RESULTS

JAK-STAT inhibition results in rapid onset of hair growth in mice

We first treated C57/B6 mice in telogen on half of the dorsal back with either vehicle control (negative control, left side), a sonic hedgehog (Shh) agonist previously shown to promote anagen initiation (*2*) (positive control), or several small-molecule inhibitors of the JAK-STAT pathway, including tofacitinib (JAK1/3 > JAK2 > TYK2) (*3*) and ruxolitinib (JAK1/2 > Tyk2 > JAK3) (*4*–*7*) (right side). As expected, entry into anagen was evident within 7 days of treatment with the Shh agonist, whereas vehicle-treated mice remained in telogen for the duration of the experiment. Intriguingly, treatment with the JAK inhibitors resulted in rapid reentry into the hair cycle, with kinetics similar to the Shh agonist (Fig. 1A). To examine a direct effect on stem cell activation, we next treated mice in telogen with tofacitinib or ruxolitinib for a short period of 4 days. Significant proliferation was noted within the hair germ compartment (P-cadherin$^+$) of drug-treated HFs (fig. S1A), indicating activation of a progenitor population. Quantification of the effects of drug treatment on skin homeostasis demonstrated that drug-induced hair growth recapitulates normal hair growth (fig. S1B). Together, these data suggest that local inhibition of the JAK-STAT pathway results in rapid onset of hair growth.

Effects of JAK-STAT inhibition are dependent on the duration of telogen

The first postnatal hair cycle in C57/B6 mice follows a precise temporal progression. Thereafter, regeneration (anagen reentry) occurs in spontaneous, patchy waves, starting around 12 to 13 weeks of age (*8*, *9*). Treatment of mice in telogen with JAK inhibitors consistently yielded early and homogeneous hair growth; however, the duration of treatment required to reinitiate anagen was inexplicably variable. To address this issue, we treated mice in early telogen (7 weeks) or mid-telogen (8.5 weeks). The treatment resulted in no growth in the 7-week-old mice, whereas 8.5-week-old mice exhibited rapid onset of anagen (fig. S1C). To ensure that mice treated at 8.5 weeks of age were still at the refractory stage of telogen that arrests the propagation of anagen reentry (*9*, *10*), we plucked hair from mice at 7 and 8.5 weeks and showed that hair growth after plucking followed a similar kinetics in both time points (fig. S1C). Notably, longer treatment of 7-week-old mice for 18 to 21 days eventually induced hair growth, but only after the treated mice had reached 8.5 weeks of age (fig. S1D). This finding implies that JAK inhibition cannot override the quiescence-promoting microenvironment at the early stages of telogen (*9*, *10*) but is sufficient to promote hair growth at a later stage in telogen.

To demonstrate the robustness and reproducibility of hair growth resulting from treatment with JAK inhibitors at 8.5 weeks of age, we took advantage of skin darkening as a proxy for hair growth in C57/B6 mice (*11*). Indeed, ~90% of 8.5-week-old mice treated with ruxolitinib or tofacitinib for 5 days displayed skin darkening and hair growth within 10 days of starting treatment, whereas no hair growth was evident in control-treated mice ($P < 0.0001$ for ruxolitinib treatment and $P = 0.04$ for tofacitinib treatment) (Fig. 1B and fig. S1E).

[1]Department of Dermatology, Columbia University, New York, NY 10032, USA. [2]Department of Systems Biology, Columbia University, New York, NY 10032, USA. [3]Department of Genetics and Development, Columbia University, New York, NY 10032, USA.
*Present address: Department of Bioengineering, Imperial College London, London SW7 2AZ, UK.
†Corresponding author. E-mail: amc65@cumc.columbia.edu

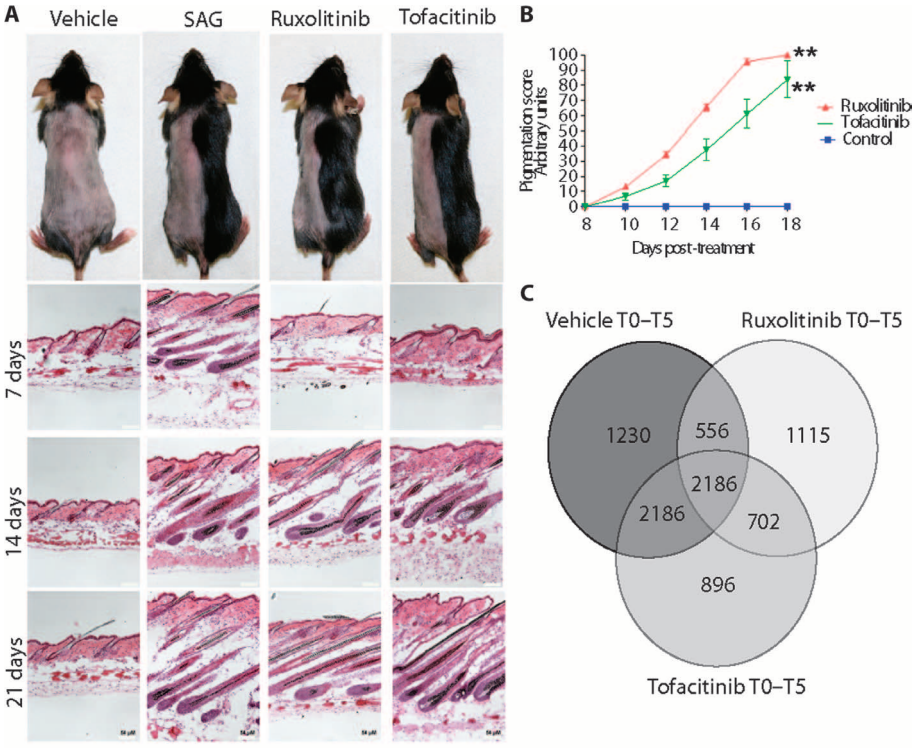

D

Category	Differentially expressed in tofacitinib and ruxolitinib T0-T5, FC > 1.5 or < 0.5, $P < 0.05$	P value
Melanogenesis	Tyrp1 Syt4 Mlana Pmel Dct Tyr Sos1 Dbf4 Pax3 PIK3ca Rps6kb1 Mlph Stx17	0.003
Wnt pathway	Acvr2a Sfrp4 Sox5 Cdh2 Fzd5 Wif1 Wnt2 Fzd8 Apc Sox9 ILK	0.017
Hair development	Shh Krt25 Dlx2 Prom1 S100a9 Vegfc Ptgfr Pdgfrl Igfbp4 Gli2	0.001

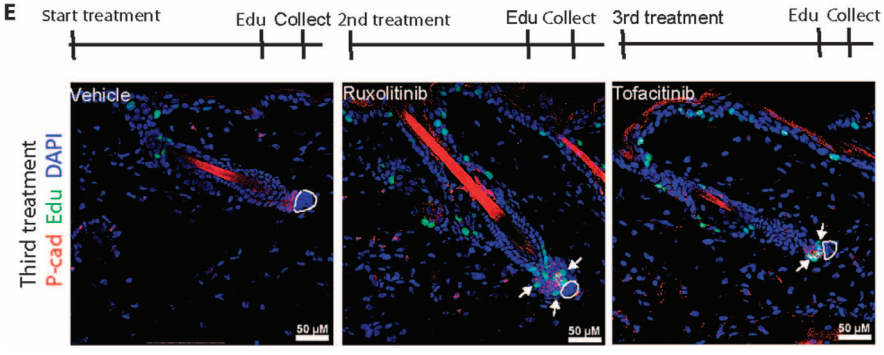

Fig. 1. Inhibition of JAK-STAT signaling restarts anagen in wild-type mice. (**A**) Seven-week-old wild-type mice were shaved and treated daily with either a topical application of vehicle control, sonic hedgehog agonist (SAG), 3% ruxolitinib (JAK1/2 inhibitor), or tofacitinib (JAK3 inhibitor). Skin was harvested at the indicated time points and stained with hematoxylin and eosin (H&E). Images of mice were taken at D21 of treatment. (**B**) Mice (8.5 weeks old) were treated with ruxolitinib, tofacitinib, or vehicle control for 5 days and were monitored for the appearance of skin pigmentation, signaling the initiation of anagen. No hair growth (and no pigmentation) was assigned the arbitrary value of 0. Skin darkening was given a value from 0 to 100%, with the higher number indicating darker skin/visible hair growth. Five mice were used per condition. Nonparametric longitudinal data analysis was performed over days 8 to 18 after treatment to generate $P = 7.6 \times 10^{-34}$ for control versus ruxolitinib and $P = 1.5 \times 10^{-10}$ for control versus tofacitinib. Double asterisks indicate high statistical significance. (**C**) Whole skin from mice treated with vehicle control, ruxolitinib, and tofacitinib for 4 days was analyzed by microarrays. Expression data were used to identify genes that were differentially expressed between T0 and T5 in each of the three treatment groups. Three mice were used per condition and biopsied at two time points. (**D**) IPA was used to identify the molecular pathways and processes that were overrepresented in our lists of differentially expressed genes. Comparison of the differentially expressed gene lists revealed a subset of genes regulated by both ruxolitinib and tofacitinib. Red, genes up-regulated in drug-treated T5 versus T0; green, genes down-regulated in drug-treated T5 versus T0. (**E**) Mice (8.5 weeks old) were treated with ruxolitinib or tofacitinib on one side of their dorsal skin and with vehicle control on the other side. Four hours after treatment, Edu was injected into each mouse, and skin was harvested 1 hour later. Treatments were performed once, twice, and thrice, and skin was analyzed for the presence of Edu^+ cells. DAPI, 4′,6-diamidino-2-phenylindole.

Hair growth after JAK-STAT inhibition mimics normal anagen initiation by activating the Wnt and Shh signaling pathways

To examine whether anagen initiation after treatment with JAK inhibitors is molecularly similar to normal anagen initiation, we performed microarray experiments on 8.5-week-old mice treated with vehicle control, ruxolitinib, or tofacitinib for 4 days, a time point at which proliferation in the hair germ has begun but hair growth is not yet evident. Comparison of the differentially expressed gene lists between whole skin harvested at day 0 (T0) and day 4 (T5) of treatment revealed a subset of genes regulated by both JAK inhibitors (Fig. 1C). Pathway analysis using Ingenuity Pathway Analysis (IPA) software showed that melanogenesis and the Wnt pathway were enriched in both ruxolitinib and tofacitinib treatments, but not in the vehicle treatment. Further analysis of differentially expressed genes in both drug treatments identified other important hair cycle regulators, such as *Shh* and *Prom1* (*2*, *12*–*16*), as significantly up-regulated in JAK inhibitor–treated skin (Fig. 1D). Differential regulation of key genes was verified by quantitative polymerase chain reaction (qPCR) (fig. S2A). Because up-regulation of Wnt and Shh pathways is central for anagen initiation and for activation of melanocyte stem cells (*16*, *17*), these findings suggest that blockade of JAK-STAT signaling allows for normal progression of the hair cycle. Further analysis of genes regulated by only one of the drug treatments revealed a distinct molecular signature (fig. S2, B and C). Ruxolitinib treatment enriched for the mTOR (mammalian target of rapamycin) and NFκB (nuclear factor κB) pathways, both previously shown to be involved in hair cycle regulation (*12*, *18*–*20*), whereas tofacitinib treatment enriched for pathways involved in cell motility and migration, such as Rho and integrin signaling. Stat3$^{-/-}$ keratinocytes were previously shown to be deficient in migration in response to stimuli (*21*, *22*), suggesting that the JAK-STAT pathway is essential for cellular motility in the transition between telogen and anagen.

JAK-STAT inhibition causes activation of HF progenitor cells

To investigate the cellular mechanisms responsible for HF activation after JAK-STAT inhibition, we treated mice in telogen with ruxolitinib, tofacitinib, or vehicle control and harvested skin 5 hours after the first, second, and third treatments (Fig. 1E, schematic). Edu (5-ethynyl-2′-deoxyuridine) was injected daily, 1 hour before harvesting each time point, and skin samples were analyzed for the presence of Edu^{+} (proliferating) cells. Edu^{+} cells are clearly visible within the hair germ (P-cadherin^{+}) compartment after three treatments in both ruxolitinib- and tofacitinib-treated skin but not in control-treated skin (Fig. 1E). This finding suggests that activation of the HF after JAK-STAT inhibition follows the normal anagen initiation kinetics, in which hair germ proliferation precedes bulge stem cell proliferation (*23*). Together, the data imply that JAK-STAT signaling normally acts to prevent anagen reentry and that JAK blockade relieves this inhibition to allow for normal hair cycle progression.

Hair-inducing effects of JAK inhibition are not dependent on the activity of lymphocytes

The JAK-STAT pathway is known to play a prominent role in T cell biology (*24*), and the HF microenvironment contains a substantial population of resident and migrating T cells. Recent studies suggested that γδ T cells secrete factors that regulate HF neogenesis in mice, as well as aspects of hair cycling (*25*, *26*). Moreover, we previously demonstrated that in AA, JAK-STAT inhibitors act to clear cytotoxic T cells from the HF microenvironment, an essential process for the onset of hair regrowth.

To evaluate whether normal hair growth after treatment with JAK inhibitors is mediated by T cells, we examined the effects of topical drug treatments on two different lymphocyte-deficient mouse models. Rag1$^{-/-}$ mice, deficient in B and T cells, and Tcr β/δ$^{-/-}$ mice, deficient in migrating and resident T cells, were largely indistinguishable from controls in terms of their ability to enter the hair cycle (fig. S3A), as well as their response to drug treatment (Fig. 2A). This suggests that the hair-inducing effects of JAK inhibitors in normal skin are not dependent on the activity of lymphocytes. Although we have not ruled out the effects of JAK-STAT inhibitors on skin macrophages (*27*) or myeloid dendritic cells (*28*), this result suggests that the anagen-inducing effects of JAK-STAT inhibition likely represent a hair-intrinsic property.

The JAK-STAT pathway is dynamically regulated across the hair cycle

To examine the kinetics of the JAK-STAT pathway in HF development and cycling, we analyzed changes in gene expression in whole skin during the transition from anagen to telogen (*29*). Using a qPCR array, we measured the expression of genes related to the JAK-STAT pathway. Dynamic changes in gene expression were visualized using Gene Expression Dynamics Inspector (GEDI), an algorithm that clusters expression values for each gene on the qPCR array into metagene categories on the basis of the similarities in their temporal expression profiles, placing them into 1 of 30 places on a 5 × 6 grid. Comparison between catagen (D17) and early anagen (D29) revealed a cluster of metagenes that became repressed as the hair cycle progressed (boxed pixels, Fig. 2B). Investigating the content of the repressed metagenes revealed that key genes in the JAK-STAT pathway such as *Stat5A/B, Stat3, Jak1, Jak3*, and *Socs2/3* were expressed at high levels in catagen and telogen and were repressed in early anagen (Fig. 2, B and C, and fig. S3B).

Immunofluorescence studies of HF in anagen, catagen, and telogen confirmed that activated (phosphorylated) Stat3 is expressed in the dermal papilla (DP), some extrafollicular cells, and the proliferating cells of the basal epidermis (Fig. 2D and fig. S3C). In catagen and telogen, phospho-Stat3 can also be detected in cells of the hair germ. Activated phospho-Stat5 is strongly expressed in the DP throughout the hair cycle, with expression peaking during catagen, where it can also be detected in the bulge (Fig. 2D). The striking expression pattern of phospho-Stat5 in key HF stem cell compartments in telogen underscores a potentially important role in regulation of quiescence.

Tofacitinib treatment promotes growth of human HFs

We next examined the effects of JAK inhibition on hair growth in human tissues. In contrast to mice, human scalp HFs grow asynchronously and 90% of them are in the anagen phase of the hair cycle at any given time (*30*). Therefore, it is extremely difficult to assess the transition between telogen to anagen in humans, and analysis is confined to measuring the rate of hair fiber elongation. Human fetal scalp skin was grafted onto SCID (severe combined immunodeficient) mice and allowed to recover for at least 6 weeks. Each graft was then treated with daily topical application of vehicle control on one side and either tofacitinib (Fig. 3A) or ruxolitinib (fig. S4A) on the other side. Small HFs were already present within the grafts, and therefore, we tested the effect of JAK inhibition on the ongoing development of fetal HFs to terminal hairs and not on HF neogenesis. Tofacitinib treatment resulted in denser HF growth as compared to controls, suggesting that tofacitinib treatment increased the rate of hair elongation. To quantify this outcome, we measured the intensity of pigmentation as a proxy for density

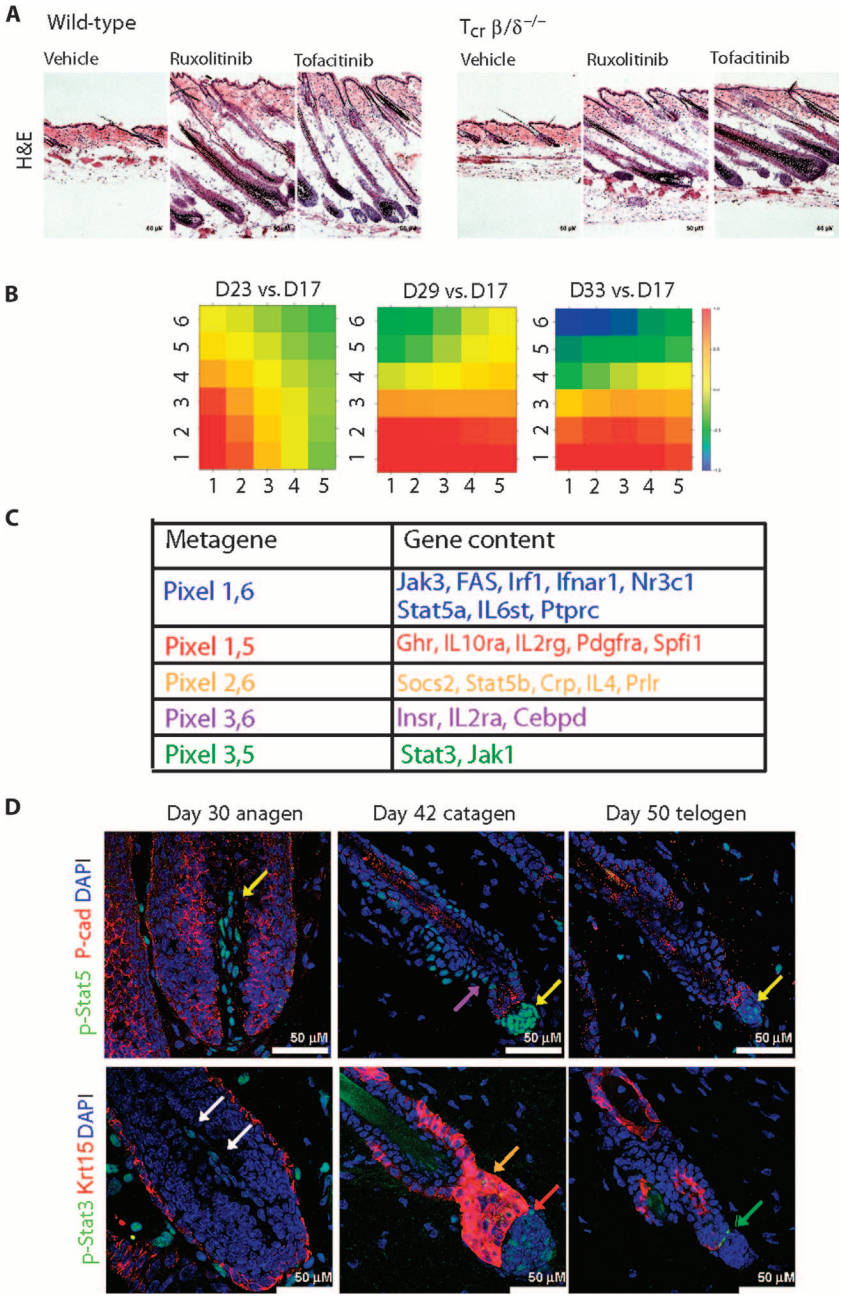

Fig. 2. The JAK-STAT pathway is dynamically regulated during HF cycling. (**A**) Eight-week-old Rag1$^{-/-}$ and Tcr β/δ$^{-/-}$ mice were treated daily with JAK inhibitors. Mice were treated for a week, and images were taken 7 days after cessation of daily treatments. Representative pictures of three mice per genotype are shown. (**B**) Whole skin was harvested from mice at postnatal day 17 (D17) (catagen), day 23 (telogen), day 29 (early anagen), and day 33 (mid-anagen). Changes in gene expression were analyzed using a JAK-STAT qPCR array that includes genes involved in the JAK-STAT pathway as well as normalizing controls (Qiagen). Three mice were used per time point, each hybridized to a separate qPCR plate. Log 2 fold changes in gene expression were used to generate GEDI self-organizing maps to visualize the dynamic changes in gene expression over the hair cycle. GEDI clusters transcripts into metagenes on the basis of their similar expression pattern over time and placed them on a 5 × 6 grid. Metagenes repressed in experimental samples (D23, D29, and D33, respectively) versus control samples (D17) are in green to blue, whereas metagenes overrepresented in experimental samples are in red. The upper and lower thresholds correspond to a twofold change. Changes larger/smaller than 2× are set to maximum color. (**C**) The gene content of the repressed metagenes highlighted in (A) (boxed pixels) is detailed in the table. The color of boxed pixels corresponds to the color of lines in the table. (**D**) Skin from wild-type mice in anagen (day 30), catagen (day 42), and telogen (D50) was harvested, fixed, and stained with anti–phospho-Stat3 (anti–p-Stat3) and anti–phospho-Stat5 (anti–p-Stat5), as well as with Krt15 (a bulge marker) and P-cadherin (hair germ marker). Phospho-Stat3 is expressed in extrafollicular cells during anagen, as well as in DP cells (white arrows). In catagen, phospho-Stat3 is expressed in the DP (red arrow) and the hair germ (orange arrow). In early telogen, phospho-Stat3 is present in the hair germ cells that are closest to the DP (green arrow). Phospho-Stat5 is strongly expressed in the DP throughout the hair cycle, with expression peaking during catagen (yellow arrows). Phospho-Stat5 can also be detected in the bulge of catagen follicles (magenta arrow). Images were taken with a Zeiss confocal microscope (×40 magnification).

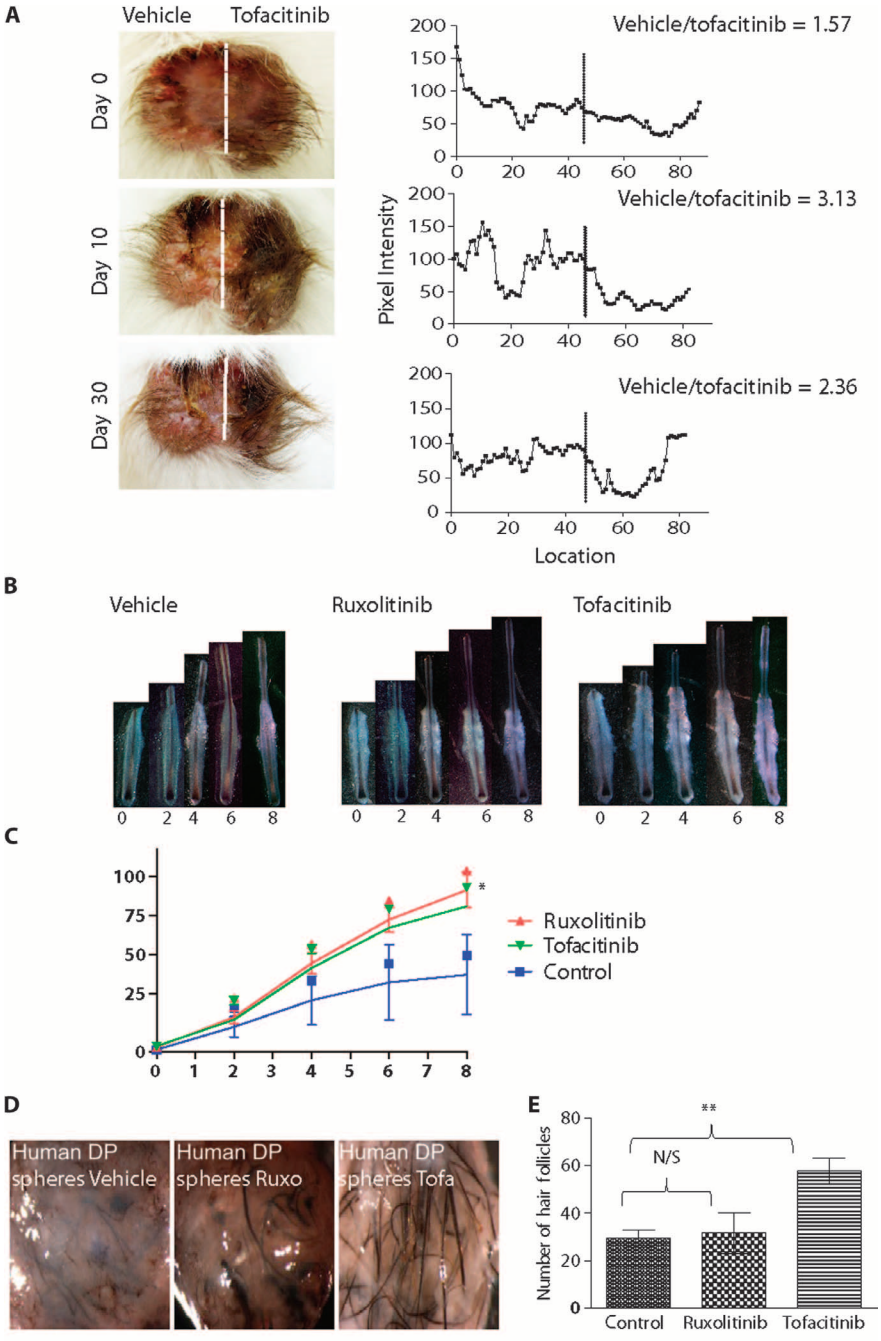

Fig. 3. Inhibition of JAK-STAT promotes hair growth in human tissue. (**A**) Human scalp skin was grafted onto *SCID* mice and topically treated with vehicle control, ruxolitinib (Ruxo), or tofacitinib (Tofa) for 4 weeks. Pictures of the grafts were taken every 3 to 5 days. To quantify differences between vehicle- and drug-treated sides, we used ImageJ to measure the intensity of pigmentation across the graft. The vertical line on each histogram corresponds to the boundary between the vehicle and drug treatments. (**B**) Individual HFs were dissected from adult human scalp tissue and placed in culture in the presence of vehicle control, ruxolitinib, and tofacitinib. Pictures of follicles were taken every 2 days for 10 days, and the length of each follicle was measured over time. (**C**) Quantification of the length of hair fibers over time. Treatment with tofacitinib and ruxolitinib significantly increased the length of hair fibers ($P = 0.017$ and $P = 0.025$, respectively). Experiment pictured was performed with follicles derived from a single donor with three to four follicles per condition. *P* values were obtained using nonparametric longitudinal data analysis. (**D**) DP spheres were grown in hanging drops in the presence of vehicle control, ruxolitinib, or tofacitinib and then combined with mouse neonatal keratinocytes and injected in vivo. Images of representative cysts are shown. (**E**) Graph of numbers of follicles induced after cysts were dissociated. Hair fibers were manually counted on a microscope. The difference between control and tofacitinib treatments is statistically significant ($P = 0.00013$). *P* values were calculated using a linear mixed-effect analysis, treating donor as a random effect. The graph represents three separate experiments with spheres generated from three individual donors. One injection of human DP spheres and mouse keratinocytes slurry was performed per DP donor per condition. N/S, not significant. Double asterisks, highly statistically significant.

of dark hairs on grafted white mice and showed that the ratio of tofacitinib/vehicle increased with days of treatment. Experiments were performed with skin derived from different donors with similar results (fig. S4B).

We further analyzed the effects of JAK inhibition on hair shaft elongation using the human HF organ culture model. Individual HFs were microdissected from human adult scalp tissue and cultured with vehicle control, ruxolitinib, and tofacitinib (Fig. 3B). We found that treatment with JAK inhibitors significantly increased the length of hair shafts when treated with ruxolitinib and tofacitinib, indicating a positive effect on the rate of hair elongation ($P = 0.023$ and $P = 0.025$ for tofacitinib and ruxolitinib, respectively). Experiments with HFs from two additional donors yielded a similar trend (fig. S4C). Together, the data suggest that JAK-STAT inhibition promotes faster hair fiber growth in the organ culture model.

Tofacitinib treatment promotes inductivity of DP

Because phospho-Stat5 is strongly expressed in mouse DP in catagen and telogen (Fig. 2D), we confirmed that phospho-STAT3 is present in the dermal sheath and DP of human HFs in anagen and phospho-STAT5 expression is weakly present in the top portion of the DP (fig. S4D).

We recently demonstrated that growing human DP cells in three-dimensional (3D) spheres improves their capacity to induce HF growth (*31*). To examine the effects of JAK inhibition on the potency of HF induction, human DP spheres were cultured with vehicle control, ruxolitinib, or tofacitinib and then combined with neonatal mouse keratinocytes and injected into nude mice. This patch assay has been shown to recapitulate HF morphogenesis and serves to evaluate trichogenic capacity (*32*). We found that tofacitinib-treated human DP spheres induced larger and significantly greater numbers of HFs overall ($P = 0.00013$) (Fig. 3D), suggesting that the inductivity of human DP is enhanced by inhibition of JAK1/3 signaling.

Tofacitinib treatment promotes hair growth by targeting genes enriched in fully inductive DP

To investigate the mechanisms by which tofacitinib treatment improves DP inductivity, we performed microarray experiments on control-, ruxolitinib-, and tofacitinib-treated DP spheres. Log 2 fold changes in gene expression were used to generate GEDI plots. To analyze relevant changes in gene expression, we compared ruxolitinib treatment (which did not confer enhanced inductivity) to controls, tofacitinib treatment (which did enhance inductivity) to controls, and ruxolitinib and tofacitinib treatments to each other. This allowed us to examine gene expression changes resulting from JAK inhibition provided by both drugs and focus on changes that were unique to tofacitinib treatment. The GEDI algorithm clustered differentially expressed transcripts into metagenes on the basis of their similar expression pattern across all microarrays. Data are presented in 3D form, where the z axis and colors correspond to changes in gene expression, and the x and y axes correspond to coordinates of GEDI metapixels, plotted on an 18×19 grid (Fig. 4A). On the basis of the topography of the graphs, we selected four regions of interest (regions 1 to 4).

Among genes that were repressed in both treatments but lower in tofacitinib treatment (region 1) were receptors known to be involved in the modulation of DP inductivity, such as FGFR1, ACVRL1, IGFR1, OSMR, and PTGFR (*33*–*38*). In the region including genes that were up-regulated by ruxolitinib treatment but down-regulated by tofacitinib treatment, we identified proapoptotic genes such as BAX, BCL2L11, and CASP12 (region 2). Genes up-regulated by tofacitinib treatment (regions 3 and 4) included members of the transforming growth factor–β (TGFβ) pathway and the bone morphogenetic protein (BMP) pathway, previously shown to play a crucial role in DP inductivity (*37*–*41*). Key regulators of the WNT pathway, such as LEF1, known to regulate dermal-epidermal interactions (*42*, *43*), and members of the NOTCH pathway known to control HF fate (*44*, *45*) were overrepresented in tofacitinib treatment. Together, this suggests that tofacitinib treatment promotes inductivity by regulating both the inductive function and the survival of cultured DP.

To directly compare tofacitinib treatment with published work on DP inductivity, we turned to our previous study, which investigated the molecular differences between freshly isolated human DP (which maintain their capacity to induce hair growth), cultured DP (which lose their inductive potential), and cultured dermal spheroids (which have restored inductive potential), and identified unique gene signatures associated with each state (*31*). These genes clustered by coexpression into four categories that we referred to as territories (T1 to T4). We found that T1 and T3 contained genes whose expression was deregulated in culture and restored by growth in spheroids, whereas T2 and T4 included genes whose expression was not restored by spheroid culture (*31*). The genes within T2 (up-regulated in cultured cells and not restored by sphere formation) and T4 (down-regulated in cultured cells and not restored by sphere formation) represent molecular signatures that appear to be required for fully inductive DP.

Since tofacitinib treatment enhanced hair growth, we assayed whether the expression of genes within T1 to T4 is enriched in a statistically significant manner, when comparing tofacitinib-treated to untreated samples. Gene set enrichment analysis (GSEA) (*46*) on genes differentially expressed in these treatment arms, ranked by P value from the highest to the lowest expression, revealed that territory T4 was significantly enriched in tofacitinib-treated spheres ($P = 2 \times 10^{-6}$; gene list provided in table S3) (Fig. 4, C and D). T2 was also enriched by tofacitinib treatment; however, the statistical overlap was only marginally significant ($P = 0.03$) (fig. S4E). Not all genes within T2 and T4 changed in the manner predicted by our previous study, suggesting that restoration of inductivity by tofacitinib treatment may not be complete. Tofacitinib treatment did up-regulate the expression of genes such as LEF1, WIF1, and CD133, all known regulators of hair growth (*37*, *38*), providing a mechanistic explanation as to why tofacitinib improved inductivity. Analysis of the ES of all JAK-STAT genes identified by the qPCR microarray used in Fig. 2B within T2 and T4 uncovered a highly statistically significant overlap (1.45×10^{-7}, gene list provided in table S1), suggesting that there is a JAK-STAT regulatory role in the T2 and T4 inductive signature.

DISCUSSION

Our findings demonstrate that inhibition of JAK-STAT signaling promotes hair growth by stimulating the activation and/or proliferation of HF stem cells, highlighting the role of this pathway in maintenance of HF quiescence. The observation that inhibition of JAK-STAT signals can promote activation or differentiation of stem/progenitor cells is not unique to the HF. Loss of Stat5 in hematopoietic stem cells induces exit from a quiescent state, leading to increased bone marrow–repopulating capacity after irradiation (*47*). Inhibition of JAK-STAT signaling improves skeletal muscle regeneration in aged mice by promoting symmetric

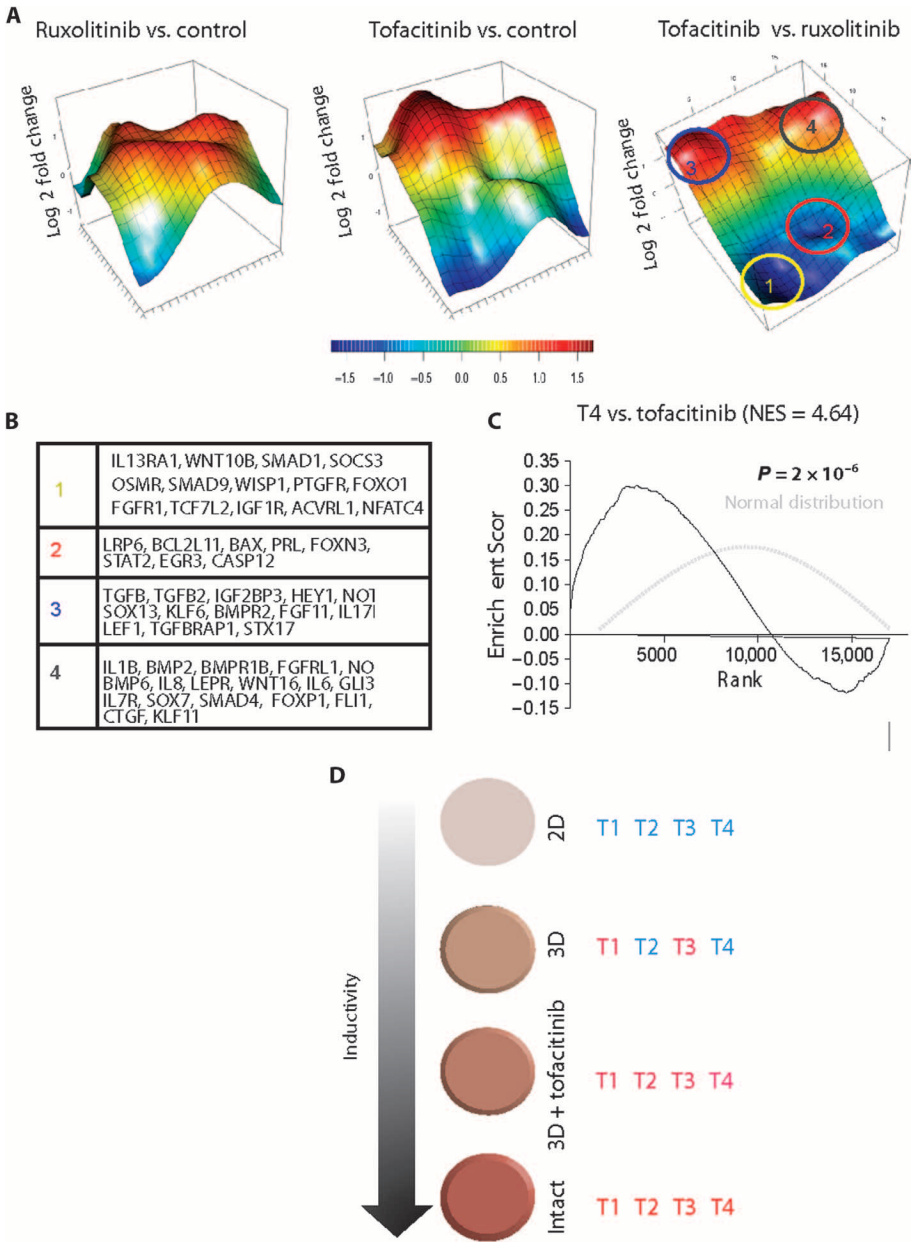

Fig. 4. Tofacitinib enhances the inductive molecular signature. (**A**) DP spheres treated with vehicle control, ruxolitinib, or tofacitinib were molecularly profiled using microarrays. Cells from three donors per condition. Log 2 fold changes in gene expression were used to generate GEDI plots visualizing the dynamic changes in gene expression over drug treatments (*z* axis and color scale). Clusters of transcripts, grouped into metagenes, were placed on an 18 × 19 grid (*x* and *y* axes). Three comparisons are shown: ruxolitinib versus control, tofacitinib versus control, and ruxolitinib versus tofacitinib. Four regions of interest are highlighted on the plots, reflecting genes repressed by tofacitinib treatment (regions 1 and 2) and genes up-regulated by tofacitinib treatment (regions 3 and 4). (**B**) Selected genes from regions 1 to 4 are presented in the table. (**C**) GSEA revealed that groups of genes previously shown to contribute to DP inductivity [genes within T2 and T4 as identified by Higgins *et al.* (*31*)] are significantly enriched by tofacitinib treatment ($P = 1.3 \times 10^{-5}$). The gray dotted line shows what a normal distribution (with no enrichment) looks like in this analysis. *X* axis describes the rank of all genes passing call in the array ranked from the most overexpressed to the most underexpressed comparing tofacitinib-treated to untreated cells. The *y* axis plots the enrichment score (ES) of the combined gene sets T2 and T4 at a given rank. The normalized ES (NES) reflects the Z-score probability of obtaining the observed ES distribution in randomized data, with the associated *P* value reported. Individual gene ranks for genes in T2 and T4 are represented as black hashes in the barcodes beneath the plot. (**D**) Summary of the results obtained in Figs. 3 and 4: Although intact DP is fully inductive, the potential to induce HF growth is lost when DP are cultured in vitro. We have previously shown that growing DP cells in spheroid cultures restores some of the inductive potential by regulating a subset of genes in the molecular signature associated with intact DP [territories 1 and 3 (T1 and T3)] (*31*). Treating DP spheres with tofacitinib increased the inductivity of cultured DP by targeting some of the pathways not previously altered by the 3D culture condition (T2 and T4). Blue, gene expression within territories corresponding on noninductive state; red, gene expression within territories corresponding to inductive state. Although tofacitinib restores genes within T2 and T4, restoration is incomplete compared to fully intact DP (territories in bright red).

satellite cell expansion and reduced commitment to myogenesis (*48*, *49*). These findings are consistent with the association of JAK-STAT with quiescence in the HF (*29*) and with evidence for a role of *Stat3* in progression of the normal hair cycle in adult mice (*21*, *22*). Moreover, recent studies have shown that increased JAK-STAT signaling in aged mice inhibits HF stem cell function in vitro (*50*) and that Stat5 signaling controls HF stem cell quiescence during pregnancy and lactation (*51*). Therefore, the role of JAK-STAT signaling in promoting quiescence may represent a generalized mechanism in adult stem cell populations.

Here, we observed that JAK inhibitor–mediated hair growth was independent of T lymphocyte function and likely represents a hair-intrinsic property. We recently demonstrated that treatment of AA patients with JAK inhibitors led to hair regrowth due in part to clearance of the $CD8^+$ $NKG2D^+$ cytotoxic T cell infiltrate but did not rule out a direct effect on the HF (*1*). These two findings are reconciled when considering hair growth in AA patients as a two-step mechanism: first, the T cell–mediated immune attack on epithelial cells must be eliminated, and second, anagen growth must be reinitiated (*52*). We observed that topical treatment with JAK inhibitors resulted in more robust hair growth than did systemic treatment in AA, likely because it increases the local concentration of drug in the HF microenvironment, allowing both actions to occur. In unaffected individuals or in normal mice, treatment with JAK inhibitors may be sufficient to restart the hair cycle (in mice) or promote hair growth (in humans).

In mice, suppression of JAK signaling activates a pro-growth/anti-quiescence signal during telogen (*9*, *53*, *54*), thereby allowing reentry into anagen. We observed that activation of the hair germ compartment containing progenitor cells is an early event in JAK inhibition–mediated hair growth and noted that pathways activated in early anagen are up-regulated after JAK inhibition. These results suggest that JAK inhibition–mediated hair growth follows the normal proliferative pattern of homeostatic hair cycling (*16*, *23*).

Anagen reentry after drug treatment occurs when mice are treated in mid-telogen but not in early telogen, suggesting that JAK inhibition cannot override the quiescence-promoting microenvironment in early telogen. Several crucial molecular events differentiate early and mid-late telogen. BMP inhibitors and Wnt agonists rise over telogen, reducing the threshold required for HF stem cell activation (*9*). Tgfβ2 and Fgf7/10 up-regulation in the DP attenuates BMP signaling in the quiescence/activation step and contributes to early anagen initiation (*23*, *41*). As telogen progresses, the hair germ up-regulates genes involved in entry into the cell cycle and signal transduction (*23*). Treatment with tofacitinib up-regulated the expression of TGFβ2, BMP6, and LEF1 in human DP spheres, providing a potential mechanism by which JAK inhibition activates the DP. We postulate that JAK inhibition of the DP (or the hair germ) is buffered by opposing signals at early stages of telogen, but as the environment becomes more permissive, the signal can induce activation. Further analysis of the molecular consequences of inhibiting JAK-STAT in the DP or the hair germ will clarify the role of this pathway in regulation of HF stem cells.

Our data suggest that JAK inhibition acts at the level of hair germ–DP crosstalk, which may occur if JAK-STAT inhibition directly targets the hair germ or, alternatively, if it targets the DP, which then activates the hair germ. We observed that phospho-Stat5 is highly expressed in the DP, suggesting potential functional importance. Moreover, by examining published microarray data from mouse hair cycle (*23*), we noted that *Jak2, Stat5A/B, Stat3,* and *Socs2/3* are all up-regulated in the DP as compared to the bulge and the hair germ. In addition, several factors involved with inhibition of hair growth or induction are highly expressed during telogen. Previous studies have shown that interleukin-6 (IL-6) and its family member oncostatin M (OSM), both of which signal via the JAK-STAT pathway, modulate hair growth. In mice, overexpression of IL-6 in keratinocytes causes retarded hair growth (*55*), and injection of recombinant IL-6 into anagen skin caused premature onset of catagen (*56*). IL-6 is also up-regulated in balding human DP versus nonbalding DP (*56*). IL-6 (*56*) and OSM (*36*) inhibit hair shaft elongation in the human organ culture model. These findings suggest that multiple pathways can activate JAK-STAT signals in different compartments, and it is likely that the dynamic interplay of these signals drives hair growth initiation.

In human hair follicle assays, we show that JAK inhibition via tofacitinib treatment increases the growth rate of anagen hair shafts (skin grafts and organotypic culture assays) and enhances the inductivity of human DP spheres (neogenesis assays). However, unlike in mice, an experimental system that directly tests human HF regeneration does not exist, so we cannot determine whether JAK inhibition drives human HF in telogen into the anagen phase. It is surprising that ruxolitinib treatment did not improve the inductivity of human DP spheres, despite the fact that it increased the rate of growth in the organ culture model. We postulate that down-regulation of proapoptotic signals in tofacitinib-treated spheres, which did not occur in ruxolitinib-treated spheres, may promote survival of DP cells, leading to enhanced hair growth in this assay. Investigation of the molecular effects of tofacitinib treatment revealed that the treatment causes a molecular restoration of a subset of genes that are disrupted in culture but are present in fully inductive DP cells (Fig. 4, C and D). This finding suggests that JAK inhibition may enhance applications such as autologous cell transplantation approaches for the treatment of hair loss.

JAK inhibitors are currently approved by the U.S. Food and Drug Administration for the treatment of myeloproliferative diseases (ruxolitinib) (*57*, *58*) and rheumatoid arthritis (tofacitinib) (*59*), and there are ongoing clinical trials demonstrating the efficacy of these drugs in treatment of psoriasis (*60*–*62*), Vitiligo (*63*), and AA (*1*, *64*, *65*). Our study raises the possibility that in addition to immune-driven conditions, JAK inhibition may prove useful in directly targeting tissue stem cells and their respective niches, opening new avenues for exploration of JAK-STAT inhibition for promoting hair growth in humans.

MATERIALS AND METHODS

Study design

We hypothesized that inhibition of JAK-STAT signaling promotes entry into the hair cycle in mice. To determine the onset of anagen, back-skin hairs were trimmed with an electric shaver, and entry of HF into anagen was observed by the appearance of darkening skin and by hair regrowth. For the hair cycle experiments described in Fig. 1A, biopsies were taken from two mice per time point, and the experiment was replicated on three sets of littermates. Data presented in the graph in Fig. 1B were generated by observing skin darkening over time after treatment, as shown in fig. S1E. For the experiments described in fig. S1 (C and D), three to four mice were used per group (7-week versus 8.5-week), and the experiment was replicated three times. For the experiment described in Fig. 1B and fig. S1E, four mice were treated with control (half of the back skin) and ruxolitinib (half of the back skin) and four mice were treated with control (half of the back skin) and tofacitinib (half of the back skin). The experiment presented in Fig. 1E

was independently replicated once, with three mice per condition. In the experiments described in Fig. 2A, three mice per genotype were used, and the experiment was replicated in two sets of littermates.

In Fig. 1 (C and D), gene expression profiling was performed on whole-skin biopsies from nine B6/C57 female mice (8.5 weeks of age). Biopsies were taken from dorsal skin at day 0 (T0) of the experiment. Mice were treated daily with dimethyl sulfoxide (DMSO), ruxolitinib, and tofacitinib on days 1 to 4, at which point a second biopsy was taken from treated mice at day 5 (T5). Quality control was performed using the affy analysisQC package from http://arrayanalysis.org/. Two samples, DMSO1 T5 and RUXO3 T5, were removed from further downstream analysis because they failed quality control. Data were normalized using the GCRMA (GC Robust Multi-array Average) method as implemented in affy analysisQC.

For Fig. 2B, skin was harvested from 3 mice per time point, and four time points were tested (12 individual mice were used for the analysis). For the human organ culture assay in Fig. 3B, follicles were derived from a single donor, and three to four follicles were used per condition. The experiment was replicated twice with follicles derived from two additional donors. For the DP sphere microarray analysis in Fig. 4A, cells were prepared from three different donors, with vehicle, ruxolitinib, and tofacitinib treatments applied to cells from each individual.

Mice

All wild-type mice in this study (adult and neonatal) are of C57/B6 background, either bred in our laboratory or purchased from the Jackson Laboratory. ICR-*SCID* mice (IcrTac:ICR-*Prkdc*^{scid}) for grafting experiments were purchased from Taconic. Athymic nude mice for the hair patch assay were purchased from Charles River. Rag1$^{-/-}$ and Tcr β/δ$^{-/-}$ mice were purchased from the Jackson Laboratory (stock nos. 002216 and 002122, respectively). All animals were maintained at the AAALAC (Accreditation of Laboratory Animal Care International) Institute for Comparative Medicine at Columbia University. Procedures were performed using Institutional Animal Care and Use Committee–approved protocols.

Human specimens

Scalp skin for grafting experiments were obtained from Advanced Bioscience Resources Inc. Occipital scalp follicles were from discarded tissue obtained during hair transplantation surgery, in accordance with the Declaration of Helsinki, after we received an exemption under 45 CFR (Code of Federal Regulations) 46 by the Institutional Review Board exemption at Columbia University.

Pharmacological inhibitors of JAK-STAT and other drugs used in this study

Ruxolitinib was purchased from ChemieTek (catalog no. CT-INCB). Tofacitinib was purchased from AbMole BioScience (catalog no. 477600-75-2). Hedgehog agonist (SAG) was purchased from EMD Millipore (catalog no. 566660). JAK-STAT inhibitors were dissolved in DMSO and used at 2 to 3% for in vivo experiments, as indicated, and 400 nM for in vitro experiments. SAG was used at 120 μM, as described by Paladini *et al.* (*2*).

Antibodies and immunofluorescence

Immunofluorescence on fresh-frozen sections of mouse skin was performed as previously described (*1*). All fluorescence images were taken with the Zeiss LSR Excited confocal microscope. All bright-field images were taken with Zeiss Axioplan 2 system. Primary antibodies used and dilutions can be found in the Supplementary Materials. Nuclei were stained using DAPI. List of antibodies is available in table S1.

Analysis of differential gene expression by qPCR array

Total RNA was isolated from mouse dorsal skin at indicated time points by using the RNeasy Mini Kit (Qiagen) in accordance with the manufacturer's instructions. Total RNA (2 μg) was reverse-transcribed with oligo(dT) primers and SuperScript III (Invitrogen). Resulting complementary DNA (cDNA) from each sample was aliquoted into a single JAK-STAT signaling qPCR array (Qiagen/SABiosciences catalog no. PAMM-039, gene list provided online). The array includes 84 genes related to the JAK-STAT pathway, plus five housekeeping genes and quality controls. Real-time PCR was performed on an ABI 7300 (Applied Biosystems). Data analysis was performed using RT^2 Profiler PCR Array data analysis software, provided by SABiosciences. Fold change in expression was determined using the $\Delta\Delta C_t$ method, and values used in downstream analysis were derived by taking the means of fold changes in three biological replicates per time point.

Gene Expression Dynamics Inspector

Values for average log 2 fold change were calculated as $-\Delta\Delta C_t$ relative to postnatal day 17 (early telogen) and were used to perform GEDI analysis to visualize how "metagenes" identified with a self-organizing map algorithm vary across samples. Metagenes are clusters of genes that show similar temporal expression patterns across samples (*66*) and that are assigned to a single pixel in a 2D grid. Neighboring pixels demonstrate similar expression patterns to one another. The self-organizing maps were then rendered using the level plot function in the lattice package in R.

Proliferation experiments

C57/B6 mice at 8.5 weeks of age were treated on half of the dorsal back with either topical vehicle control (left side) or JAK inhibitors (right side). Four hours after treatment, each mouse received a single injection of Edu (20 mg/kg) (Invitrogen). One hour after injection, skin was harvested, fixed and stained using the Click-iT EdU Alexa Fluor 488 Imaging Kit (Life Technologies) per the manufacturer's instructions, and costained for P-cadherin. Experiment was replicated once, with one mouse per time point.

Microarray analysis

Total RNA was extracted using the Qiagen RNeasy Micro Kit. The Ovation RNA Amplification kit (Nugen) was used to generate amplified cDNA for microarray analysis. Arrays used were Affymetrix mouse 430 2.0, hybridized at the Columbia University Medical Center microarray facility. qPCR analysis was performed on the ABI 7300 cycler. Primer sequences are available in table S2. LIMMA (Linear Models for Microarray Data) was used with a multilevel model to identify genes that were differentially expressed between samples at T5 and T0 for each treatment group (DMSO, RUXO, and TOFA) using a threshold of fold change of 1.5 and $P < 0.05$. Results from the differential expression analysis were uploaded to IPA to identify the molecular pathways that were overrepresented in each of the lists of differentially expressed genes for each of our treatment groups.

For the DP sphere microarray analysis, total RNA was extracted from DP spheres cultured in DMSO, ruxolitinib, or tofacitinib from each of the three donors using the Qiagen RNeasy Micro Kit. The Ovation

RNA Amplification kit (Nugen) was used to generate amplified cDNA for microarray analysis. LIMMA was used with a linear model treating both treatment and the blocking factor donor as fixed effects. Contrasts of interest between treatments were used to identify genes that were differentially expressed between pairs of treatments for the treatments DMSO, RUXO, and TOFA. A threshold of absolute fold change of 1.5 and $P < 0.05$ was used. For GSEA, the HG_U133_Plus_2.0 chip annotation file downloaded from ftp://ftp.broad.mit.edu//pub/gsea/annotations/ was used to annotate the Affymetrix probe sets and to remove duplicate probe sets for a given gene symbol. Duplicates were removed on the basis of the maximum absolute fold change observed for each gene symbol. Preranked gene lists were generated for each treatment contrast of interest using the moderated *t*-statistics returned by LIMMA. GSEA was performed on these lists to identify KEGG (Kyoto Encyclopedia of Genes and Genomes) pathways overrepresented in each list (ES, $P = 0.01$).

Gene set enrichment analysis

The GSEA comparing tofacitinib-treated and control cells was performed by generating a list of all detected transcripts ranked by differential expression (*P* value) and direction of fold change (up or down). This ranked list was tested for the enrichment of the union of territories 2 and 4 (gene list provided in table S3) as previously described (*31*). A null distribution for computing the NES and its associated *P* value was obtained by label shuffling to randomize the gene rankings. These randomized sets were then used to compute null ESs over 5000 iterations to generate a null distribution. The observed leading-edge ES was normalized to this distribution, and a two-tailed *P* value was generated for this NES.

Human HF organ culture assay

Adult human follicles were microdissected from occipital skin under sterile conditions as previously described. Individual follicles were placed in a 24-well tissue culture plate in Williams E medium supplemented with hydrocortisone, insulin, and glutamine (*67*) in the presence of DMSO, ruxolitinib, or tofacitinib (400 nM). Medium was replaced every 2 days, and images of individual follicles were taken every 2 days. Analysis of the growth rate of each follicle was performed using ImageJ.

Patch assay with DP spheres

DP cells were grown in spheres as previously described (*31*). DMSO, ruxolitinib, or tofacitinib was added to the medium (400 nM). Each hanging drop contained 1000 cells, which aggregated to form DP spheroids after 24 hours. Forty-eight hours after plating, 500 spheres in each condition were collected for use in the patch assay. Each experiment was performed with cells derived from a single individual, and four separate experiments were conducted. Keratinocytes were isolated from newborn mice by following the protocol outlined by Lichti *et al.* (*68*). Cells were cultured in defined keratinocyte serum-free medium for 2 to 4 days before being harvested for the patch assay. Newborn murine keratinocytes (1×10^6) were then mixed together with 500 human DP spheres in each condition and subdermally injected into dorsal skin of a nude mouse. Twelve days after performing the injections, cysts had developed in the dermis, some of which contained HF and hair fibers. These cysts were collected, photographed, and then digested in 0.35% collagenase. The digested slurries were spread onto microscope slides, and hair fiber counts were manually performed under a stereo microscope.

Human skin grafting assay

Human scalp skin (16 weeks old), about 2 × 2 cm in diameter, was grafted onto the back of SCID mice. The mice were bandaged, and the grafts were left to recover for 6 weeks. After 6 weeks, small hairs could be observed on the grafts. Grafts were treated daily with topical application of vehicle control, ruxolitinib, or tofacitinib. Treatment continued for 4 weeks, and pictures were taken every 3 to 5 days. Experiments were performed with skin from three separate donors.

Quantification of hair growth was performed using ImageJ. Taking advantage of the fact that the donor hair was dark and the grafted mouse was white, we measured the intensity of pigmentation as a proxy for density of HF. Because the control and experimental treatments were performed on the same graft, each image allows for direct comparison between the vehicle- and drug-treated skin. Intensity was scored across three lines per image and averaged to generate the histograms shown in Fig. 3A and fig. S4A. Darker regions are given a lower value than bright regions. Ratio was calculated by averaging the intensity values for the control-treated side by the intensity values for the drug-treated side, accounting for pretreatment differences in hair growth on the graft and for changes in hair density occurring over time.

Statistical analysis

A significance level of $P = 0.05$ was used for all tests. For both the organ culture longitudinal study (Fig. 3, B and C) and the skin pigmentation study (Fig. 1B), nonparametric longitudinal data analysis was performed using the R package nparLD to test the hypothesis that a treatment-by-time interaction exists, that is, time profiles are not parallel, for comparisons of pairs of treatments. In the organ culture study, an F1-LD-F1 design was used. In the skin pigmentation study, an LD-F2 model was performed for the ruxolitinib versus control and tofacitinib versus control comparisons to account for the paired design, and an F1-LD-F1 model was used for the tofacitinib versus ruxolitinib comparison because the data were unpaired. The analysis of variance (ANOVA)–type statistic was tested for significance at $\alpha = 0.05$ (a randomized complete block design was used to analyze the human DP sphere patch assay) (Fig. 3E). Three treatments each were applied to DP spheres from each of three donors. Donor was treated as a fixed blocking factor. The unit of statistical analysis is the number of observed HFs. The data were analyzed using a linear mixed-effects model treating the blocking factor donor as a random effect. The R packages lme4 and lmerTest were used to test whether the fixed factor treatment significantly contributed to the number of follicles observed and to perform post hoc comparisons of treatment means. The package lmerTest used the Satterthwaite approximation to obtain *P* values and denominator degrees of freedom.

SUPPLEMENTARY MATERIALS

Supplementary material for this article is available at http://advances.sciencemag.org/cgi/content/full/1/9/e1500973/DC1

Fig. S1. JAK inhibition–mediated hair growth recapitulates endogenous hair growth and is dependent on the duration of telogen.

Fig. S2. Molecular pathways enriched in genes differentially regulated by each JAK-STAT inhibitor.

Fig. S3. Effects of JAK inhibition are independent of T cells and instead represent cell-intrinsic properties.

Fig. S4. Inhibition of JAK-STAT promotes human HF growth.

Table S1. List of antibodies and dilutions used in this study.

Table S2. List of qPCR primers used in this study.

Table S3. List of genes within territories T2 and T4 [as adapted from Higgins *et al.* (*31*)].

REFERENCES AND NOTES

1. L. Xing, Z. Dai, A. Jabbari, J. E. Cerise, C. A. Higgins, W. Gong, A. de Jong, S. Harel, G. M. DeStefano, L. Rothman, P. Singh, L. Petukhova, J. Mackay-Wiggan, A. M. Christiano, R. Clynes, Alopecia areata is driven by cytotoxic T lymphocytes and is reversed by JAK inhibition. *Nat. Med.* **20**, 1043–1049 (2014).
2. R. D. Paladini, J. Saleh, C. Qian, G.-X. Xu, L. L. Rubin, Modulation of hair growth with small molecule agonists of the hedgehog signaling pathway. *J. Invest. Dermatol.* **125**, 638–646 (2005).
3. M. Cutolo, The kinase inhibitor tofacitinib in patients with rheumatoid arthritis: Latest findings and clinical potential. *Ther. Adv. Musculoskelet. Dis.* **5**, 3–11 (2013).
4. T Zhou, S. Georgeon, R. Moser, D. J. Moore, A. Caflisch, O. Hantschel, Specificity and mechanism-of-action of the JAK2 tyrosine kinase inhibitors ruxolitinib and SAR302503 (TG101348). *Leukemia* **28**, 404–407 (2014).
5. R. A. Mesa, U. Yasothan, P. Kirkpatrick, Ruxolitinib. *Nat. Rev. Drug Discov.* **11**, 103–104 (2012).
6. D. C. Borie, J. J. O'Shea, P. S. Changelian, JAK3 inhibition, a viable new modality of immunosuppression for solid organ transplants. *Trends Mol. Med.* **10**, 532–541 (2004).
7. S. Verstovsek, R. A. Mesa, J. Gotlib, R. S. Levy, V. Gupta, J. F. DiPersio, J. V. Catalano, M. Deininger, C. Miller, R. T. Silver, M. Talpaz, E. F. Winton, J. H. Harvey Jr., M. O. Arcasoy, E. Hexner, R. M. Lyons, R. Paquette, A. Raza, K. Vaddi, S. Erickson-Viitanen, I. L. Koumenis, W. Sun, V. Sandor, H. M. Kantarjian, A double-blind, placebo-controlled trial of ruxolitinib for myelofibrosis. *N. Engl. J. Med.* **366**, 799–807 (2012).
8. S. Müller-Röver, B. Handjiski, C. van der Veen, S. Eichmüller, K. Foitzik, I. A. McKay, K. S. Stenn, R. Paus, A comprehensive guide for the accurate classification of murine hair follicles in distinct hair cycle stages. *J. Invest. Dermatol.* **117**, 3–15 (2001).
9. M. V. Plikus, J. A. Mayer, D. de la Cruz, R. E. Baker, P. K. Maini, R. Maxson, C.-M. Chuong, Cyclic dermal BMP signalling regulates stem cell activation during hair regeneration. *Nature* **451**, 340–344 (2008).
10. M. V. Plikus, R. E. Baker, C.-C. Chen, C. Fare, D. de la Cruz, T. Andl, P. K. Maini, S. E. Millar, R. Widelitz, C.-M. Chuong, Self-organizing and stochastic behaviors during the regeneration of hair stem cells. *Science* **332**, 586–589 (2011).
11. L. Alonso, E. Fuchs, The hair cycle. *J. Cell Sci.* **119**, 391–393 (2006).
12. R. Schmidt-Ullrich, D. J. Tobin, D. Lenhard, P. Schneider, R. Paus, C. Scheidereit, NF-κB transmits Eda A1/EdaR signalling to activate Shh and cyclin D1 expression, and controls post-initiation hair placode down growth. *Development* **133**, 1045–1057 (2006).
13. I. Brownell, E. Guevara, C. B. Bai, C. A. Loomis, A. L. Joyner, Nerve-derived Sonic hedgehog defines a niche for hair follicle stem cells capable of becoming epidermal stem cells. *Cell Stem Cell* **8**, 552–565 (2011).
14. W.-M. Woo, H. H. Zhen, A. E. Oro, Shh maintains dermal papilla identity and hair morphogenesis via a Noggin–Shh regulatory loop. *Genes Dev.* **26**, 1235–1246 (2012).
15. Y. Ito, T. S. Hamazaki, K. Ohnuma, K. Tamaki, M. Asashima, H. Okochi, Isolation of murine hair-inducing cells using the cell surface marker prominin-1/CD133. *J. Invest. Dermatol.* **127**, 1052–1060 (2007).
16. Y.-C. Hsu, L. Li, E. Fuchs, Transit-amplifying cells orchestrate stem cell activity and tissue regeneration. *Cell* **157**, 935–949 (2014).
17. P. Rabbani, M. Takeo, W. Chou, P. Myung, M. Bosenberg, L. Chin, M. M. Taketo, M. Ito, Coordinated activation of Wnt in epithelial and melanocyte stem cells initiates pigmented hair regeneration. *Cell* **145**, 941–955 (2011).
18. R. M. Castilho, C. H. Squarize, L. A. Chodosh, B. O. Williams, J. S. Gutkind, mTOR mediates Wnt-induced epidermal stem cell exhaustion and aging. *Cell Stem Cell* **5**, 279–289 (2009).
19. A. J. Kellenberger, M. Tauchi, Mammalian target of rapamycin complex 1 (mTORC1) may modulate the timing of anagen entry in mouse hair follicles. *Exp. Dermatol.* **22**, 77–80 (2013).
20. R. Schmidt-Ullrich, T. Aebischer, J. Hülsken, W. Birchmeier, U. Klemm, C. Scheidereit, Requirement of NF-κB/Rel for the development of hair follicles and other epidermal appendices. *Development* **128**, 3843–3853 (2001).
21. S. Sano, S. Itami, K. Takeda, M. Tarutani, Y. Yamaguchi, H. Miura, K. Yoshikawa, S. Akira, J. Takeda, Keratinocyte-specific ablation of Stat3 exhibits impaired skin remodeling, but does not affect skin morphogenesis. *EMBO J.* **18**, 4657–4668 (1999).
22. S. Sano, M. Kira, S. Takagi, K. Yoshikawa, J. Takeda, S. Itami, Two distinct signaling pathways in hair cycle induction: Stat3-dependent and -independent pathways. *Proc. Natl. Acad. Sci. U.S.A.* **97**, 13824–13829 (2000).
23. V. Greco, T. Chen, M. Rendl, M. Schober, H. A. Pasolli, N. Stokes, J. dela Cruz-Racelis, E. Fuchs, A two-step mechanism for stem cell activation during hair regeneration. *Cell Stem Cell* **4**, 155–169 (2009).
24. A. Ferrajoli, S. Faderl, F. Ravandi, Z. Estrov, The JAK-STAT pathway: A therapeutic target in hematological malignancies. *Curr. Cancer Drug Targets* **6**, 671–679 (2006).
25. D. Gay, O. Kwon, Z. Zhang, M. Spata, M. V. Plikus, P. D. Holler, M. Ito, Z. Yang, E. Treffeisen, C. D. Kim, A. Nace, X. Zhang, S. Baratono, F. Wang, D. M. Ornitz, S. E. Millar, G. Cotsarelis, Fgf9 from dermal γδ T cells induces hair follicle neogenesis after wounding. *Nat. Med.* **19**, 916–923 (2013).
26. J. E. Kloepper, K. Kawai, M. Bertolini, T. Kanekura, R. Paus, Loss of γδ T cells results in hair cycling defects. *J. Invest. Dermatol.* **133**, 1666–1669 (2013).
27. D. Castellana, R. Paus, M. Perez-Moreno, Macrophages contribute to the cyclic activation of adult hair follicle stem cells. *PLOS Biol.* **12**, e1002002 (2014).
28. A. Heine, S. A. E. Held, S. Nora Daecke, S. Wallner, S. Parampalli Yajnanarayana, C. Kurts, D. Wolf, P. Brossart, The JAK-inhibitor ruxolitinib impairs dendritic cell function in vitro and in vivo. *Blood* **122**, 1192–1202 (2013).
29. K. K. Lin, D. Chudova, G. W. Hatfield, P. Smyth, B. Andersen, Identification of hair cycle-associated genes from time-course gene expression profile data by using replicate variance. *Proc. Natl. Acad. Sci. U.S.A.* **101**, 15955–15960 (2004).
30. K. S. Stenn, R. Paus, Control of hair follicle cycling. *Physiol. Rev.* **81**, 449–494 (2001).
31. C. A. Higgins, J. C. Chen, J. E. Cerise, C. A. Jahoda, A. M. Christiano, Microenvironmental reprogramming by three-dimensional culture enables dermal papilla cells to induce de novo human hair-follicle growth. *Proc. Natl. Acad. Sci. U.S.A.* **110**, 19679–19688 (2013).
32. Y. Zheng, X. Du, W. Wang, M. Boucher, S. Parimoo, K. Stenn, Organogenesis from dissociated cells: Generation of mature cycling hair follicles from skin-derived cells. *J. Invest. Dermatol.* **124**, 867–876 (2005).
33. R. R. Driskell, A. Giangreco, K. B. Jensen, K. W. Mulder, F. M. Watt, Sox2-positive dermal papilla cells specify hair follicle type in mammalian epidermis. *Development* **136**, 2815–2823 (2009).
34. M. Kawano, A. Komi-Kuramochi, M. Asada, M. Suzuki, J. Oki, J. Jiang, T. Imamura, Comprehensive analysis of FGF and FGFR expression in skin: FGF18 is highly expressed in hair follicles and capable of inducing anagen from telogen stage hair follicles. *J. Invest. Dermatol.* **124**, 877–885 (2005).
35. H. Kamp, C. C. Geilen, C. Sommer, U. Blume-Peytavi, Regulation of PDGF and PDGF receptor in cultured dermal papilla cells and follicular keratinocytes of the human hair follicle. *Exp. Dermatol.* **12**, 662–672 (2003).
36. M. Yu, S. Kissling, P. Freyschmidt-Paul, R. Hoffmann, J. Shapiro, Interleukin-6 cytokine family member oncostatin M is a hair-follicle-expressed factor with hair growth inhibitory properties. K. J. McElwee, *Exp. Dermatol.* **17**, 12–19 (2008).
37. M. Rendl, L. Lewis, E. Fuchs, Molecular dissection of mesenchymal–epithelial interactions in the hair follicle. *PLOS Biol.* **3**, e331 (2005).
38. M. Rendl, L. Polak, E. Fuchs, BMP signaling in dermal papilla cells is required for their hair follicle-inductive properties. *Genes Dev.* **22**, 543–557 (2008).
39. R. Paus, K. Foitzik, P. Welker, S. Bulfone-Paus, S. Eichmüller, Transforming growth factor-β receptor type I and type II expression during murine hair follicle development and cycling. *J. Invest. Dermatol.* **109**, 518–526 (1997).
40. K. Foitzik, R. Paus, T. Doetschman, G. P. Dotto, The TGF-β2 isoform is both a required and sufficient inducer of murine hair follicle morphogenesis. *Dev. Biol.* **212**, 278–289 (1999).
41. N. Oshimori, E. Fuchs, Paracrine TGF-β signaling counterbalances BMP-mediated repression in hair follicle stem cell activation. *Cell Stem Cell* **10**, 63–75 (2012).
42. P. Zhou, C. Byrne, J. Jacobs, E. Fuchs, Lymphoid enhancer factor 1 directs hair follicle patterning and epithelial cell fate. *Genes Dev.* **9**, 700–713 (1995).
43. K. Kratochwil, M. Dull, I. Farinas, J. Galceran, R. Grosschedl, *Lef1* expression is activated by BMP-4 and regulates inductive tissue interactions in tooth and hair development. *Genes Dev.* **10**, 1382–1394 (1996).
44. B. Hu, K. Lefort, W. Qui, B.-C. Nguyen, R. D. Rajaram, E. Castillo, F. He, Y. Chen, P. Angel, C. Brisken, G. P. Dotto, Control of hair follicle cell fate by underlying mesenchyme through a CSL–Wnt5a–FoxN1 regulatory axis. *Genes Dev.* **24**, 1519–1532 (2010).
45. C. A. Ambler, F. M. Watt, Expression of Notch pathway genes in mammalian epidermis and modulation by β-catenin. *Dev. Dyn.* **236**, 1595–1601 (2007).
46. A. Subramanian, P. Tamayo, V. K. Mootha, S. Mukherjee, B. L. Ebert, M. A. Gillette, A. Paulovich, S. L. Pomeroy, T. R. Golub, E. S. Lander, J. P. Mesirov, Gene set enrichment analysis: A knowledge-based approach for interpreting genome-wide expression profiles. *Proc. Natl. Acad. Sci. U.S.A.* **102**, 15545–15550 (2005).
47. Z. Wang, G. Li, W. Tse, K. D. Bunting, Conditional deletion of STAT5 in adult mouse hematopoietic stem cells causes loss of quiescence and permits efficient nonablative stem cell replacement. *Blood* **113**, 4856–4865 (2009).
48. F. D. Price, J. von Maltzahn, C. F. Bentzinger, N. A. Dumont, H. Yin, N. C. Chang, D. H. Wilson, J. Frenette, M. A. Rudnicki, Inhibition of JAK-STAT signaling stimulates adult satellite cell function. *Nat. Med.* **20**, 1174–1181 (2014).
49. M. T. Tierney, T. Aydogdu, D. Sala, B. Malecova, S. Gatto, P. L. Puri, L. Latella, A. Sacco, STAT3 signaling controls satellite cell expansion and skeletal muscle repair. *Nat. Med.* **20**, 1182–1186 (2014).
50. J. Doles, M. Storer, L. Cozzuto, G. Roma, W. M. Keyes, Age-associated inflammation inhibits epidermal stem cell function. *Genes Dev.* **26**, 2144–2153 (2012).
51. J. Goldstein, S. Fletcher, E. Roth, C. Wu, A. Chun, V. Horsley, Calcineurin/Nfatc1 signaling links skin stem cell quiescence to hormonal signaling during pregnancy and lactation. *Genes Dev.* **28**, 983–994 (2014).
52. S. J. Divito, T. S. Kupper, Inhibiting Janus kinases to treat alopecia areata. *Nat. Med.* **20**, 989–990 (2014).

53. E. Festa, J. Fretz, R. Berry, B. Schmidt, M. Rodeheffer, M. Horowitz, V. Horsley, Adipocyte lineage cells contribute to the skin stem cell niche to drive hair cycling. *Cell* **146**, 761–771 2011).
54. C. A. B. Jahoda, A. M. Christiano, Niche crosstalk: Intercellular signals at the hair follicle. *Cell* **146**, 678–681 (2011).
55. K. Turksen, T. Kupper, L. Degenstein, I. Williams, E. Fuchs, Interleukin 6: Insights to its function in skin by overexpression in transgenic mice. *Proc. Natl. Acad. Sci. U.S.A.* **89**, 5068–5072 (1992).
56. M. H. Kwack, J. S. Ahn, M. K. Kim, J. C. Kim, Y. K. Sung, Dihydrotestosterone-inducible IL-6 inhibits elongation of human hair shafts by suppressing matrix cell proliferation and promotes regression of hair follicles in mice. *J. Invest. Dermatol.* **132**, 43–49 (2012).
57. A. Quintás-Cardama, K. Vaddi, P. Liu, T. Manshouri, J. Li, P. A. Scherle, E. Caulder, X. Wen, Y. Li, P. Waeltz, M. Rupar, T. Burn, Y. Lo, J. Kelley, M. Covington, S. Shepard, J. D. Rodgers, P. Haley, H. Kantarjian, J. S. Fridman, S. Verstovsek, Preclinical characterization of the selective JAK1/2 inhibitor INCB018424: Therapeutic implications for the treatment of myeloproliferative neoplasms. *Blood* **115**, 3109–3117 (2010).
58. H. L. Geyer, R. A. Mesa, Therapy for myeloproliferative neoplasms: When, which agent, and how? *Blood* **124**, 3529–3537 (2014).
59. K. Ghoreschi, M. I. Jesson, X. LI, J. L. Lee, S. Ghosh, J. W. Alsup, J. D. Warner, M. Tanaka, S. M. Steward-Tharp, M. Gadina, C. J. Thomas, J. C. Minnerly, C. E. Storer, T. P. LaBranche, Z. A. Radi, M. E. Dowty, R. D. Head, D. M. Meyer, N. Kishore, J. J. O'Shea, Modulation of innate and adaptive immune responses by tofacitinib (CP-690,550). *J. Immunol.* **186**, 4234–4243 (2011).
60. H. Bachelez, P. C. van de Kerkhof, R. Strohal, A. Kubanov, F. Valenzuela, J. H. Lee, V. Yakusevich, S Chimenti, J. Papacharalambous, J. Proulx, P. Gupta, H. Tan, M. Tawadrous, H. Valdez, R. Wolk, Tofacitinib versus etanercept or placebo in moderate-to-severe chronic plaque psoriasis: A phase 3 randomised non-inferiority trial. *Lancet* **386**, 552–561 (2015).
61. N. Punwani, T. Burn, P. Scherle, R. Flores, J. Shi, P. Collier, D. Hertel, P. Haley, Y. Lo, P. Waeltz, J. Rodgers, S. Shepard, K. Vaddi, S. Yeleswaram, R. Levy, W. Williams, A. B. Gottlieb, Down-regulation of key inflammatory cell markers with topical Janus kinase 1/2 inhibitor. *Br. J. Dermatol.*, 10.1111/bjd.13994 (2015).
62. L. L. Levy, J. Urban, B. A. King, Treatment of reclacitrant atopic dermatitis with the oral Janus kinase inhibitor tofacitinib citrate. *J. Am. Acad. Dermatol.* **73**, 395–399 (2015).
63. B. G. Craiglow, B. A. King, Tofacitinib citrate for the treatment of vitiligo: A pathogenesis-directed therapy. *JAMA Dermatol.* 10.1001/jamadermatol.2015.1520 (2015).
64. B. G. Craiglow, B. A. King, Killing two birds with one stone: Oral tofacitinib reverses alopecia universalis in a patient with plaque psoriasis. *J. Invest. Dermatol.* **134**, 2988–2990 (2014).
65. A. Jabbari, Z. Dai, L. Xing, J. E. Cerise, Y. Ramot, Y. Berkun, G. A. Sanchez, R. Goldbach-Mansky, A. M. Christiano, R. Clynes, A. Zlotogorski, Reversal of alopecia areata following treatment with the JAK1/2 inhibitor baricitinib. *EBioMedicine* **4**, 351–355 (2015).
66. G. S. Eichler, S. Huang, D. E. Ingber, Gene Expression Dynamics Inspector (GEDI): For integrative analysis of expression profiles. *Bioinformatics* **19**, 2321–2322 (2003).
67. D. J. Tobin, *Ex Vivo Organ Culture of Human Hair Follicles: A Model Epithelial–Neuroectodermal–Mesenchymal Interaction System* (Methods in Molecular Biology Series, Humana Press, New York, 2011), vol. 695, pp. 213–227.
68. U. Lichti, J. Anders, S. H. Yuspa, Isolation and short-term culture of primary keratinocytes, hair follicle populations and dermal cells from newborn mice and keratinocytes from adult mice for in vitro analysis and for grafting to immunodeficient mice. *Nat. Protoc.* **3**, 799–810 (2008).

Acknowledgments: We thank D. Owens for advice and technical assistance, A. De Jong and E. Wang for their valuable comments on the manuscript, and E. Chang and M. Zhang for their help with animal experiments. **Funding:** This work was supported in part by U.S. Public Health Service NIH National Institute of Arthritis and Musculoskeletal and Skin Diseases grants R01AR056016 (to A.M.C.), R21AR061881 (to A.M.C. and R.C.), and P30AR044535 (the Columbia University Skin Disease Research Center), as well as the Locks of Love Foundation and the Alopecia Areata Initiative. S.H. was funded with the Dermatology Foundation Career Development Award. J.E.C. and J.C.C. were supported by the Kirschstein National Research Service Award postdoctoral training grant in Medical Genetics [T32GM082271 (to A.M.C.)]. **Author contributions:** S.H., C.A.H., Z.D., R.C., and A.M.C. contributed to the conception and design of the study. S.H., C.A.H., J.E.C., J.C.C., and Z.D. contributed to data collection, analysis, and interpretation. S.H. and A.M.C. drafted the report. All authors approved the final version of the report. **Competing interests:** Columbia University has filed patent applications relating to the discoveries reported in this paper, which are being commercialized through Vixen Pharmaceuticals Inc., of which A.M.C. is a founder. The other authors declare that they have no competing interests. **Data and materials availability:** Microarray data were deposited in Gene Expression Omnibus and will be available upon publication of the article.

Submitted 22 July 2015
Accepted 30 July 2015
Published 23 October 2015
10.1126/sciadv.1500973

Citation: S. Harel, C. A. Higgins, J. E. Cerise, Z. Dai, J. C. Chen, R. Clynes, A. M. Christiano, Pharmacologic inhibition of JAK-STAT signaling promotes hair growth. *Sci. Adv.* **1**, e1500973 (2015).

ScienceAdvances
AAAS

Pharmacologic inhibition of JAK-STAT signaling promotes hair growth

Sivan Harel, Claire A. Higgins, Jane E. Cerise, Zhenpeng Dai, James C. Chen, Raphael Clynes and Angela M. Christiano

(October 23, 2015)
Sci Adv 2015, 1:.
doi: 10.1126/sciadv.1500973